Available online at www.sciencedirect.com
SCIENCE DIRECT®
Comput. Methods Appl. Mech. Engrg. 192 (2003) 2501–2519
Computer methods in applied mechanics and engineering
www.elsevier.com/locate/cma

The nearly-optimal Petrov–Galerkin method for convection–diffusion problems

Ali Nesliturk [a], Isaac Harari [b,*]

[a] Department of Mathematics, Izmir Institute of Technology, 35437 Izmir, Turkey
[b] Department of Solid Mechanics, Materials and Systems, Tel Aviv University, 69978 Ramat Aviv, Israel

Received 10 April 2001; accepted 27 September 2002

Abstract

The nearly-optimal Petrov–Galerkin (NOPG) method is employed to improve finite element computation of convection-dominated transport phenomena. The design of the NOPG method for convection–diffusion is based on consideration of the advective limit. Nonetheless, the resulting method is applicable to the entire admissible range of problem parameters. An investigation of the stability properties of this method leads to a coercivity inequality. The convergence features of the NOPG method for convection–diffusion are studied in an error analysis that is based on the stability estimates. The proposed method compares favorably to the performance of an established technique on several numerical tests.

1. Introduction

The standard finite element method is based on continuous, piecewise polynomial, Galerkin approximation. This approach is optimal for the Laplace operator in the sense that it minimizes the error in the energy norm—the H^1 semi-norm in this case. In geometric terms, the finite element solution is the projection of the exact solution on the finite element function space. This property is referred to as best approximation, and it assures good performance of the computation at any mesh refinement, i.e., high coarse-mesh accuracy.

However, good numerical performance at any mesh resolution is not guaranteed by the standard finite element method for other cases. Consequently, finite element computation can become prohibitively expensive in the presence of sharp gradients and rapid oscillations. For example, the Galerkin finite element method with low-order piecewise polynomials performs poorly for advection-dominated equations.

* Corresponding author. Tel.: +972-3-640-9439; fax: +972-3-640-7617.
E-mail address: harari@eng.tau.ac.il (I. Harari).

0045-7825/03/$ - see front matter
doi:10.1016/S0045-7825(03)00269-X

Numerous approaches to alleviating these difficulties have been proposed. Inevitably, these are based on modifications of the classical piecewise polynomial Galerkin approximation. Among these approaches we note Galerkin/least-squares [13] and related stabilized methods (SUPG/SD [5] and USFEM [7], see also [10]), residual-free bubbles (RFB) [4,9], (see also [8]) variational multi-scale (VMS) [11,15], the generalized finite element method (GFEM) [17], based on the partition of unity method (PUM) [1,14], the discontinuous enrichment method (DEM) [6], and nearly-optimal Petrov–Galerkin (NOPG) [2].

NOPG, previously developed as a general methodology and applied to the Helmholtz equation [2], is motivated by the desire to achieve high coarse-mesh accuracy via best approximation in the H^1 semi-norm, in order to guarantee good performance of the computation at any mesh refinement. Practical considerations lead to a Petrov–Galerkin formulation which *approximates* H^1 optimality [2]. In some cases, such as piecewise linear basis functions on regular meshes, the NOPG formulation yields results that are identical to those obtained by RFB.

In this paper we apply the NOPG method to problems of convection–diffusion. The NOPG method as a general approach for improving finite element computation is reviewed in Section 2, and the method is then specialized to convection–diffusion problems. In Section 3 we investigate stability features of the NOPG method for the convection-dominated case. The analysis is similar to that of RFB [4,9]. We prove the convergence of NOPG for convection–diffusion in Section 4. The numerical performance of the proposed method and of established techniques are compared in Section 5.

2. Formulation

Let $\Omega \subset \mathbb{R}^d$ be a d-dimensional, open, bounded region with smooth boundary Γ.

2.1. Boundary-value problem

For simplicity, we consider the following homogeneous Dirichlet boundary-value problem: Find $u : \overline{\Omega} \to \mathbb{R}$ such that

$$\mathscr{L}u = f \quad \text{in } \Omega, \tag{1}$$

$$u = 0 \quad \text{on } \Gamma, \tag{2}$$

where $f : \Omega \to \mathbb{R}$ is a given function. We think of $\mathscr{L}$ as a second-order differential operator. The generalization to boundary-value problems with other types of boundary conditions and inhomogeneous boundary data is straightforward (see Section 5 for numerical results with other types of boundary conditions).

2.2. Weak form

The variational form of the boundary-value problem (1) and (2) is stated in terms of the set of functions $\mathscr{V} = H_0^1(\Omega)$. We seek $u \in \mathscr{V}$ such that

$$a(v, u) = (v, f), \quad \forall v \in \mathscr{V}. \tag{3}$$

Here

$$a(v, u) = (v, \mathscr{L}u) = (\mathscr{L}^* v, u) \tag{4}$$

for all sufficiently smooth u, $v \in \mathscr{V}$ and assuming sufficiently smooth f; $(\cdot, \cdot)$ is the $L_2(\Omega)$ inner product. Subscripts on inner products denote domains of integration other than Ω.

2.3. Petrov–Galerkin approximation

In the following presentation we review the original derivation of NOPG [2] for completeness.

The conventional approximation, by the Galerkin method, is obtained by finding $v^h \in \mathscr{V}^h \subset \mathscr{V}$ such that

$$a(v^h, u^h) = (v^h, f), \quad \forall v^h \in \mathscr{V}^h, \tag{5}$$

$\mathscr{V}^h$ is a conventional finite dimensional finite element space. The approximation u^h that results from (5), however, is not necessarily optimal in any sense.

Instead, we wish to consider an alternative approach. We seek an approximation to u which is optimal in terms of the H^1 semi-norm. That is, we wish to find $u^h \in \mathscr{V}^h$ such that

$$(\nabla v^h, \nabla e) = 0, \quad \forall v^h \in \mathscr{V}^h. \tag{6}$$

Here $e = u^h - u$ and u is solution of (1) and (2) or (3). Generally, (6) cannot be solved for u^h, since u is unknown. However, for the special case when $\mathscr{L} = -\Delta$, the Galerkin approximation (5) leads to the H^1 projection (6), which guarantees good performance of the computation on any mesh refinement. Our goal, then, is to formulate a problem that retains optimality in the sense of (6), at least approximately, yet may be solved directly.

Partition Ω in the usual way into n_{el} non-overlapping regions Ω_e (element domains) with boundaries Γ_e, $e = 1, \ldots, n_{\mathrm{el}}$ (see Fig. 1). We denote the union of element interiors by

$$\widetilde{\Omega} = \bigcup_{e=1}^{n_{\mathrm{el}}} \Omega_e. \tag{7}$$

Similarly, the union of element boundaries is denoted

$$\widetilde{\Gamma} = \bigcup_{e=1}^{n_{\mathrm{el}}} \Gamma_e. \tag{8}$$

We assume that $\mathscr{V}^h$ is given. Then, for each Galerkin weighting function $v^h \in \mathscr{V}^h$, we construct a function $\bar{v}^h \in \bar{\mathscr{V}}^h \subset \mathscr{V}$ that satisfies

$$\mathscr{L}^* \bar{v}^h = \Delta v^h \quad \text{in } \widetilde{\Omega}, \tag{9}$$

$$\bar{v}^h = v^h \quad \text{on } \widetilde{\Gamma}. \tag{10}$$

We note that while the functions $v_{\mathrm{b}} = \bar{v}^h - v^h$ are bubbles over the elements, they are not residual free, except in special cases such as piecewise linear Galerkin weighting functions on regular meshes.

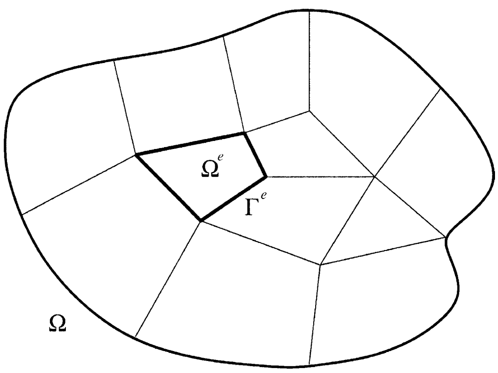

Fig. 1. Domain Ω partitioned into element domains Ω_e.

Starting from the H^1 projection (6), we now derive our NOPG formulation:

$$(\nabla v^h, \nabla e) = -(\nabla^2 v^h, e)_{\tilde{\Omega}} + ([v^h_{,n}], e)_{\tilde{\Gamma}} = -(\mathscr{L}^* \bar{v}^h, e)_{\tilde{\Omega}} + ([v^h_{,n}], e)_{\tilde{\Gamma}} = a(\bar{v}^h, e) + ([v^h_{,n} - \bar{v}^h_{,n}], e)_{\tilde{\Gamma}}$$
$$= a(\bar{v}^h, u^h) - (\bar{v}^h, f) + ([v^h_{,n} - \bar{v}^h_{,n}], e)_{\tilde{\Gamma}}, \tag{11}$$

where we have used integration by parts, the definition of weight functions (9) and the fact that $\bar{\mathscr{V}}^h \subset \mathscr{V}$. Here, $[\cdot]$ is the jump at an element boundary. Eq. (11) motivates the following NOPG problem: Find $u^h \in \mathscr{V}$ such that

$$a(\bar{v}^h, u^h) = (\bar{v}^h, f), \quad \forall \bar{v}^h \in \bar{\mathscr{V}}^h. \tag{12}$$

The term 'nearly-optimal' can be justified by the fact that this formulation approximates the H^1-optimal result (6), in the sense that its solution satisfies

$$(\nabla v^h, \nabla e) = ([v^h_{,n} - \bar{v}^h_{,n}], e)_{\tilde{\Gamma}}. \tag{13}$$

The non-zero right-hand side is a measure of the distance of the Petrov–Galerkin solution from H^1-optimality. This is related to the lack of symmetry of the formulation.

In practice, the Petrov–Galerkin weighting functions $\bar{v}^h$ may be defined in terms of the bubbles v_b. Using integration by parts and the vanishing trace of the bubbles on element boundaries, the NOPG variational equation (12) is then computed as

$$a(v^h, u^h) + (v_b, \mathscr{L} u^h)_{\tilde{\Omega}} = (v^h + v_b, f). \tag{14}$$

We now apply the method to the convection–diffusion equation.

2.4. The NOPG method for convection–diffusion

Convection–diffusion describes many transport phenomena and serves as a model for fluid mechanics. Let $\mathscr{L}$ be the convection–diffusion operator, i.e.,

$$\mathscr{L} = -\kappa \Delta + \boldsymbol{a} \cdot \nabla. \tag{15}$$

The diffusivity $\kappa(\boldsymbol{x}) > 0$ is known and $\boldsymbol{a}(\boldsymbol{x})$ is the given flow velocity. In this case

$$a(\bar{v}^h, u^h) = (\nabla \bar{v}^h, \kappa \nabla u^h) + (\bar{v}^h, \boldsymbol{a} \cdot \nabla u^h). \tag{16}$$

in the NOPG formulation (12).

In order to complete the definition of the method, we consider a discrete space $\mathscr{V}^h$ containing piecewise linears on triangles. The Petrov–Galerkin weighting functions $\bar{v}^h$ are designed via the bubbles v_b, which satisfy the following BVP:

$$\mathscr{L}^* v_b = -\mathscr{L}^* v^h \quad \text{in } \widetilde{\Omega}, \tag{17}$$

$$v_b = 0 \quad \text{on } \widetilde{\Gamma}, \tag{18}$$

since $\mathscr{L}^*$ is linear, $\mathscr{L}^* \bar{v}^h = \triangle v^h$ by (9) and (10) and $\triangle v^h = 0$ for linear triangles.

In practice, our current implementation of the method is based on a simplification of v_b that is obtained by considering a reduced solution at the advective limit. Nonetheless, the resulting method is applicable in the entire range from diffusion-dominated to advection-dominated cases (see the numerical tests in Section 5).

For each triangle Ω_e, let $\Gamma_e^+ = \{\boldsymbol{x} \in \Gamma_e : \boldsymbol{a} \cdot \boldsymbol{n}(\boldsymbol{x}) > 0\}$ be its outflow boundary and $\Gamma_e^- = \{\boldsymbol{x} \in \Gamma_e : \boldsymbol{a} \cdot \boldsymbol{n}(\boldsymbol{x}) < 0\}$ its inflow boundary, where $\boldsymbol{n}$ is the outward-pointing unit normal to Γ_e. Assume that $\boldsymbol{a} \cdot \boldsymbol{n}(\boldsymbol{x})$ is bounded away from zero; then, excluding vertices, for each Ω_e we have $\Gamma_e = \Gamma_e^- \cup \Gamma_e^+$. As $\kappa \to 0$, the problem (17) and (18) reduces to finding the reduced solution v_b^0:

$$-\boldsymbol{a}\cdot\nabla v_{\mathrm{b}}^{0}=\boldsymbol{a}\cdot\nabla v^{h}\quad\text{in }\Omega_{e},\tag{19}$$

$$v_{\mathrm{b}}^{0}=0\quad\text{on }\Gamma_{e}^{+}.\tag{20}$$

Let $(\boldsymbol{x}^-,\boldsymbol{x}^+)$ be a generic line segment that lies parallel to $\boldsymbol{a}$ in a single element domain with $\boldsymbol{x}^-\in\Gamma_e^-$ and $\boldsymbol{x}^+\in\Gamma_e^+$. The solution for (19) and (20) is simply

$$v_{\mathrm{b}}^{0}(\boldsymbol{x})=v^{h}(\boldsymbol{x}^{+})-v^{h}(\boldsymbol{x}),\quad\text{for }\boldsymbol{x}\in(\boldsymbol{x}^{-},\boldsymbol{x}^{+}).\tag{21}$$

We may think of v_{b}^{0} as a modification of (21) that contains a thin boundary layer along the inflow boundary Γ_e^-, in order to satisfy consistency requirements. The presence of such a boundary layer is of little consequence in the integration of the bubble multiplying the inner-element residual, see (14), so that it may be neglected in practice.

In summary, our method is implemented as the NOPG variational equation (12), with the bilinear operator (16), and the Petrov–Galerkin weighting functions $\bar{v}^h=v^h+v_{\mathrm{b}}^0$, where v_{b}^0 is given in (21).

3. Stability of the NOPG method for convection–diffusion

In this section, we investigate stability features of the NOPG method for the convection–diffusion equation. We are primarily interested in the case where the discrete space $\mathscr{V}^h$ is the space of piecewise linears on triangles. We further assume the advection $\boldsymbol{a}$ is piecewise constant inside each element. Thus $\boldsymbol{a}\cdot\nabla v^h$ is constant in each element and $\triangle v^h=0$ throughout the domain $\widetilde{\Omega}$ in this case.

Stability of the diffusion-dominated case is evident. In the following we focus on the convection-dominated case where $\kappa\ll 1$. To prove that the bilinear form (16) is coercive over $\bar{\mathscr{V}}^h\times\mathscr{V}^h$, assume that κ is constant within each element and substitute $\bar{v}^h=v^h+v_{\mathrm{b}}$ into (16):

$$\begin{aligned}a(\bar{v}^h,v^h)&=\sum_e\left(\kappa(\nabla\bar{v}^h,\nabla v^h)_{\Omega_e}+(\bar{v}^h,\boldsymbol{a}\cdot\nabla v^h)_{\Omega_e}\right)\\&=\sum_e\left(\kappa|v^h|_{1,\Omega_e}^2+\kappa(\nabla v^h,\nabla v_{\mathrm{b}})_{\Omega_e}+(v^h,\boldsymbol{a}\cdot\nabla v^h)_{\Omega_e}+(v_{\mathrm{b}},\boldsymbol{a}\cdot\nabla v^h)_{\Omega_e}\right)\\&=\sum_e\left(\kappa|v^h|_{1,\Omega_e}^2+(v_{\mathrm{b}},\boldsymbol{a}\cdot\nabla v^h)_{\Omega_e}\right).\end{aligned}\tag{22}$$

In order to obtain the last line in (22) we integrated by parts and used the facts that $v^h=0$ on the boundary of Ω, $v_{\mathrm{b}}=0$ on each Γ_e, $\boldsymbol{a}$ is constant and $\Delta v^h=0$ on each Ω_e since v^h is linear.

Case I. *Limiting case* $\kappa\to 0$. In this case we employ the reduced solution (21)

$$v_{\mathrm{b}}^{0}(\boldsymbol{x})=v^{h}(\boldsymbol{x}^{+})-v^{h}(\boldsymbol{x}),\quad\text{for }\boldsymbol{x}\in(\boldsymbol{x}^{-},\boldsymbol{x}^{+})=\frac{1}{|\boldsymbol{a}|}\int_{\boldsymbol{x}}^{\boldsymbol{x}^+}\boldsymbol{a}\cdot\nabla v^h(s)\,\mathrm{d}s=\frac{1}{|\boldsymbol{a}|}(\boldsymbol{a}\cdot\nabla v^h)|_{\Omega_e}|\boldsymbol{x}^+-\boldsymbol{x}|\tag{23}$$

since $\boldsymbol{a}\cdot\nabla v^h$ is constant in each element.

By the formula for the volume of the pyramid we observe that

$$\int_K|\boldsymbol{x}^+-\boldsymbol{x}|\,\mathrm{d}x=\frac{h_a|K|}{3},$$

where $\boldsymbol{x}\in(\boldsymbol{x}^-,\boldsymbol{x}^+)$ and h_a is defined as the length of the longest segment parallel to the flow and contained in Ω_e (see Fig. 2).

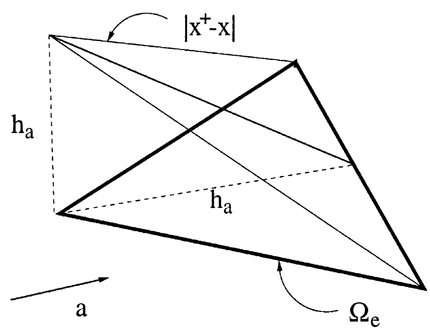

Fig. 2. The region below the surface $z = |\boldsymbol{x}^+ - \boldsymbol{x}|$ is a pyramid.

Hence, recalling (22) and taking into account that $\kappa \to 0$, we get

$$a(\bar{v}^h, v^h) = \sum_e (\kappa |v^h|^2_{1,\Omega_e} + (v^0_{\mathrm{b}}, \boldsymbol{a} \cdot \nabla v^h)_{\Omega_e}), \tag{24}$$

$$= \sum_e \left(\kappa |v^h|^2_{1,\Omega_e} + \frac{h_a}{|3\boldsymbol{a}|} \|\boldsymbol{a} \cdot \nabla v^h\|^2_{\Omega_e} \right). \tag{25}$$

The expression in the second term can be shown to be weaker than the semi-norm that appears in the standard analysis of the streamline upwind Petrov–Galerkin (SUPG) method when parameters are chosen as in [7].

Case II. $0 < \kappa \ll 1$

The coercivity result can be extended to the case where $0 < \kappa \ll 1$ and $\mathscr{V}^h$ is the space of piecewise linears on triangles Ω_e. Rewriting (22) and using the result obtained in Case 1, we get

$$a(\bar{v}^h, v^h) = \sum_e (\kappa |v^h|^2_{1,\Omega_e} + (v_{\mathrm{b}}, \boldsymbol{a} \cdot \nabla v^h)_{\Omega_e}),$$

$$= \sum_e (\kappa |v^h|^2_{1,\Omega_e} + (v^0_{\mathrm{b}}, \boldsymbol{a} \cdot \nabla v^h)_{\Omega_e} + (v_{\mathrm{b}} - v^0_{\mathrm{b}}, \boldsymbol{a} \cdot \nabla v^h)_{\Omega_e}),$$

$$= \sum_e \left(\kappa |v^h|^2_{1,\Omega_e} + \frac{h_a}{|3\boldsymbol{a}|} \|\boldsymbol{a} \cdot \nabla v^h\|^2_{\Omega_e} + (v_{\mathrm{b}} - v^0_{\mathrm{b}}, \boldsymbol{a} \cdot \nabla v^h)_{\Omega_e} \right). \tag{26}$$

To obtain coercivity, we need to prove that the third term in this sum is dominated by the second term. This can be achieved by the virtue of the following lemma.

Lemma 1. *Let Ω_e be a fixed triangle in our triangulation. Suppose that no edge in the triangulation is aligned with the direction of the flow and that $v_{\mathrm{b}} - v^0_{\mathrm{b}}$ is defined on Ω_e by*

$$\begin{cases} \mathscr{L}^*(v_{\mathrm{b}} - v^0_{\mathrm{b}}) = \kappa \Delta v^0_{\mathrm{b}} & \text{in } \Omega_e, \\ v_{\mathrm{b}} - v^0_{\mathrm{b}} = 0 & \text{on } \Gamma^+_e, \\ v_{\mathrm{b}} - v^0_{\mathrm{b}} = v^h(\boldsymbol{x}^-) - v^h(\boldsymbol{x}^+) & \text{on } \Gamma^-_e. \end{cases} \tag{27}$$

Then there exists a fixed positive constant C, which is independent of κ, h_a and $|\boldsymbol{a}|$, such that

$$\|v_{\mathrm{b}} - v^0_{\mathrm{b}}\|_{0,\Omega_e} \leqslant C \left(\frac{\kappa^{1/2} h_a^{1/2}}{|\boldsymbol{a}|^{3/2}} + \frac{\kappa}{|\boldsymbol{a}|^2} \right) \|\boldsymbol{a} \cdot \nabla v^h\|_{0,\Omega_e}.$$

Proof. Proof of the lemma follows the lines of [9]. For notational convenience, set $z = v_b - v_b^0$. Define the function Φ on Ω_e, letting $\phi(\boldsymbol{x}) = v^h(\boldsymbol{x}^+) - v^h(\boldsymbol{x})$, by

$$\begin{cases} \mathscr{L}^*\Phi = 0 & \text{in } \Omega_e, \\ \Phi = 0 & \text{on } \Gamma_e^+, \\ \Phi = \phi(\boldsymbol{x}^-) & \text{on } \Gamma_e^-, \end{cases}$$

so that Φ is a smooth boundary-layer-like extension of ϕ over Ω_e. Now set $w = z - \Phi$. Then

$$\begin{cases} \mathscr{L}^*w = \kappa\Delta v_b^0 & \text{in } \Omega_e, \\ w = 0 & \text{on } \Gamma_e. \end{cases}$$

If Γ_e^+ is a single side of Ω_e, then $\kappa\Delta v_b^0 = 0$ on Ω_e, and then $w = 0$ all over the domain Ω_e implying $z = \Phi$ but in general this is not the case. Therefore we assume that Γ_e^+ consists of two edges of Ω_e (see Fig. 3).

Let us denote the cartesian coordinates in two dimensions by (x, y). Since $\boldsymbol{a}$ is constant on Ω_e, without loss of generality we assume that $\boldsymbol{a} = a_1\vec{\mathbf{e}}_1$ for some $a_1 > 0$, where $\vec{\mathbf{e}}_1$ is the unit vector in the direction of the positive x-axis.

We first bound w in terms of the crosswind derivative of v_b^0. Then develop an argument to bound the crosswind derivative of v_b^0 in terms of streamline derivative of this function.

Choose $(x^*, y^*) \in \Gamma_e^-$ such that $x^* \leqslant x$ for all $(x, y) \in \Omega_e$ (see Fig. 4). Multiply $\mathscr{L}^*w = \kappa\Delta v_b^0$ by $(x - x^*)w(x, y)$ and integrate over Ω_e, to get

$$\begin{aligned} \int_{\Omega_e} (x - x^*)(\mathscr{L}^*w)(x, y)w(x, y)\,\mathrm{d}x\,\mathrm{d}y &= \int_{\Omega_e} \left[\kappa(x - x^*)|\nabla w(x, y)|^2 + \frac{a_1}{2}(x - x^*)\frac{\partial}{\partial x}w^2(x, y)\right]\mathrm{d}x\,\mathrm{d}y \\ &= \int_{\Omega_e} [\kappa(x - x^*)|\nabla w(x, y)|^2 + (a_1/2)w^2(x, y)]\,\mathrm{d}x\,\mathrm{d}y, \end{aligned} \tag{28}$$

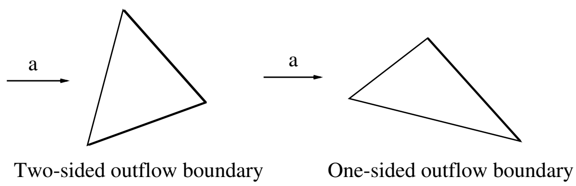

Fig. 3. Types of outflow boundary.

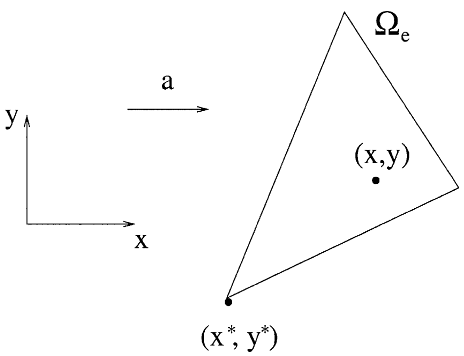

Fig. 4. The point (x^*, y^*) is the leftmost point in Ω_e.

where we integrated by parts and used $w=0$ on Γ_e. Next, integrating the left-hand side of (28) by parts and using the inequality

$$\boldsymbol{a}\cdot\boldsymbol{b} \leqslant \frac{|\boldsymbol{a}|^2+|\boldsymbol{b}|^2}{2},$$

we get

$$\begin{aligned}\int_{\Omega_e}(x-x^*)(\kappa\Delta v_{\mathrm{b}}^0)(x,y)w(x,y)\,\mathrm{d}x\,\mathrm{d}y &= \int_{\Omega_e}\kappa\nabla v_{\mathrm{b}}^0(x,y)\cdot\nabla((x-x^*)w(x,y))\,\mathrm{d}x\,\mathrm{d}y\\ &= \int_{\Omega_e}\kappa\nabla v_{\mathrm{b}}^0(x,y)\cdot((x-x^*)\nabla w(x,y)-w(x,y)\vec{\mathbf{e}}_1)\,\mathrm{d}x\,\mathrm{d}y\\ &\leqslant \frac{1}{2}\int_{\Omega_e}\left[\kappa(x-x^*)|\nabla w(x,y)|^2+\frac{a_1}{2}w^2(x,y)\right]\mathrm{d}x\,\mathrm{d}y\\ &\quad+\frac{1}{2}\int_{\Omega_e}\left[\kappa(x-x^*)|\nabla v_{\mathrm{b}}^0(x,y)|^2+\frac{2\kappa^2}{a_1}|\nabla v_{\mathrm{b}}^0(x,y)|^2\right]\mathrm{d}x\,\mathrm{d}y. \qquad (29)\end{aligned}$$

Combining (28) and (29), we have

$$\begin{aligned}\frac{1}{2}\int_{\Omega_e}\frac{a_1}{2}w^2(x,y)\,\mathrm{d}x\,\mathrm{d}y &\leqslant \frac{1}{2}\int_{\Omega_e}\left[\kappa(x-x^*)|\nabla w(x,y)|^2+\frac{a_1}{2}w^2(x,y)\right]\mathrm{d}x\,\mathrm{d}y\\ &\leqslant \frac{1}{2}\int_{\Omega_e}\left[\kappa(x-x^*)|\nabla v_{\mathrm{b}}^0(x,y)|^2+\frac{2\kappa^2}{a_1}|\nabla v_{\mathrm{b}}^0(x,y)|^2\right]\mathrm{d}x\,\mathrm{d}y.\end{aligned}$$

Consequently, we infer that

$$\int_{\Omega_e}w^2(x,y)\,\mathrm{d}x\,\mathrm{d}y \leqslant \frac{4}{a_1}\int_{\Omega_e}\left(\kappa(x-x^*)+\frac{2\kappa^2}{a_1}\right)|\nabla v_{\mathrm{b}}^0(x,y)|^2\,\mathrm{d}x\,\mathrm{d}y \leqslant \frac{4}{a_1}\int_{\Omega_e}\left(\kappa h_a+\frac{2\kappa^2}{a_1}\right)|\nabla v_{\mathrm{b}}^0(x,y)|^2\,\mathrm{d}x\,\mathrm{d}y.$$

Thus

$$\|w\|_{0,\Omega_e} \leqslant 2\left(\frac{\kappa^{1/2}h_a^{1/2}}{a_1^{1/2}}+\frac{\sqrt{2}\kappa}{a_1}\right)\|\nabla v_{\mathrm{b}}^0\|_{0,\Omega_e}. \qquad (30)$$

We now bound $\|\nabla v_{\mathrm{b}}^0\|_{0,\Omega_e}$ in terms of its streamline derivative. Recall that we assume that Γ_e^+ consists of two edges of Ω_e and the edges of each Ω_e are bounded away from being parallel to $\boldsymbol{a}=a_1\vec{\mathbf{e}}_1$. This means that we can write the equations of the two edges E_1 and E_2 in Γ_e^+ as $x^+=m_jy+k_j$ for each $j\in\{1,2\}$, where the m_j and k_j are constants that satisfy $|m_j|\leqslant C_1$ for some fixed constant C_1.

If (x,y) lies in the part of Ω_e that is upwind to a point (x^+,y) on the side E_j, $j\in\{1,2\}$, then, letting $\Lambda=(1/|\boldsymbol{a}|)(\boldsymbol{a}\cdot\nabla v^h)|_{\Omega_e}$, from (23) we have

$$v_{\mathrm{b}}^0(x,y)=\Lambda|x^+-x|=\Lambda(x^+-x)=\Lambda((m_jy+k_j)-x),$$

since $\boldsymbol{a}=a_1\vec{\mathbf{e}}_1$ and $a_1>0$. Then it is easy to see that

$$\left|\frac{\partial v_{\mathrm{b}}^0(x,y)}{\partial y}\right| = |\Lambda m_j| \leqslant C_1|\Lambda| = C_1\left|\frac{\partial v_{\mathrm{b}}^0(x,y)}{\partial x}\right|.$$

(This inequality bounds the cross-wind derivative of v_{b}^0 in terms of the streamline derivative of this function.) Hence,

$$\|\nabla v_{\mathrm{b}}^0\|_{0,\Omega_e} \leqslant \|(v_{\mathrm{b}}^0)_x\|_{0,\Omega_e}+\|(v_{\mathrm{b}}^0)_y\|_{0,\Omega_e} \leqslant ((1+C_1)/a_1)\|\boldsymbol{a}\cdot\nabla v_{\mathrm{b}}^0\|_{0,\Omega_e} = ((1+C_1)/a_1)\|\boldsymbol{a}\cdot\nabla v^h\|_{0,\Omega_e},$$

where we have used (19). Invoking this inequality in (30), we obtain

$$\|w\|_{0,\Omega_e} \leqslant 2(1+C_1)\left(\frac{\kappa^{1/2}h_a^{1/2}}{a_1^{3/2}}+\frac{\sqrt{2}\kappa}{a_1^2}\right)\|\boldsymbol{a}\cdot\nabla v^h\|_{0,\Omega_e}. \tag{31}$$

Next we bound $\|\Phi\|_{0,\Omega_e}$. As an application of maximum principle for the advection–diffusion operator, this will be accomplished by designing a suitable barrier function for Φ: A function such that if it satisfies $|\Phi|\leqslant\theta$ on Γ_e and $|L\Phi|\leqslant L\theta$ on Ω_e then $|\Phi|\leqslant\theta$ on all of Ω_e; see [16]. At the end, an upper bound for the barrier function will also be the desired bound for Φ.

We shall do this for the case where Γ_e^- consists of two edges of Ω_e; the case where Γ_e^- is a single edge is similar but easier.

Let the two edges in Γ_e^- be E_1 and E_2, where the equation of E_j is $x_j^- = m_j'y + k_j'$ for $j=\{1,2\}$, and the m_j' and k_j' are constants. Extend each edge E_j to form a complete line (which we still call E_j, see Fig. 5). Given $(x,y)\in\Omega_e$, define $x_j^- = x_j^-(x,y)$ by the requirement that (x_j^-,y) lie on E_j (see Fig. 6).

We set M and N such that

$$M = \max_{\Gamma_e^-}\{|\phi|\},$$

$$N = 1 + (m_1')^2 + (m_2')^2.$$

Define the function $\theta_j(x,y)$ by

$$\theta_j(x,y) = M\mathrm{e}^{-a_1(x-x_j^-)/(\kappa N)} \geqslant 0, \quad \text{for } j\in\{1,2\}.$$

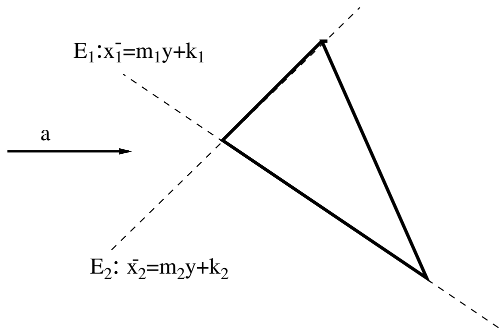

Fig. 5. $x - x_j^-$ is always non-negative inside the triangle.

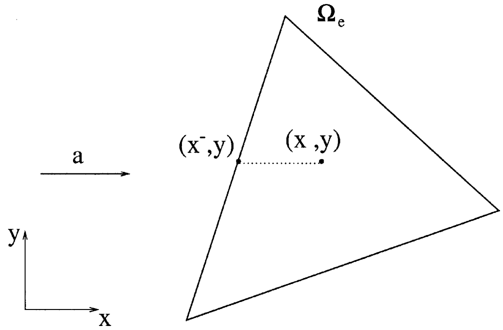

Fig. 6. The point (x,y) is upwind to (x_j^-,y) in the streamline direction.

Observe that

$$\begin{cases} \theta_j = M & \text{on } E_j, \\ \theta_j \leqslant M & \text{on } \Gamma_e^- \setminus E_j, \\ \theta_j \leqslant M & \text{in } \Omega_e, \end{cases} \tag{32}$$

For each j, a calculation shows that

$$\mathscr{L}^* \theta_j(x, y) = \frac{a_1^2}{\kappa N} \left(1 - \frac{1 + (m'_j)^2}{N}\right) \theta_j \geqslant 0,$$

since $N \geqslant 1 + (m'_j)^2$. Now set $\theta(x, y) = \theta_1(x, y) + \theta_2(x, y)$. Then

$$\mathscr{L}^* \theta = \mathscr{L}^* \theta_1 + \mathscr{L}^* \theta_2 \geqslant 0 = \mathscr{L}^* \Phi$$

on Ω_e, and if $(x, y) \in \Gamma_e^-$, then

$$\theta(x^-) = \theta_1(x^-) + \theta_2(x^-) > M \geqslant \Phi(x^-) = \phi(x^-),$$

because, by construction, $\theta_j = M$ on E_j; also $\theta > 0 = \Phi$ on Γ_e^+. That is, we have shown that θ is a barrier function for Φ on Ω_e. The maximum principle now implies that $|\Phi| \leqslant \theta$ on Ω_e. We make use of the well-known inequality

$$(a + b)^2 \leqslant 2(a^2 + b^2) \quad \text{for all } a, b \in \mathbb{R},$$

to estimate the norm of Φ by the barrier function:

$$\begin{aligned}
\|\Phi\|_{0,\Omega_e} \leqslant \|\theta\|_{0,\Omega_e} &= \|\theta_1 + \theta_2\|_{0,\Omega_e} \\
&\leqslant \left\{ \int_{\Omega_e} \left(M \mathrm{e}^{-a_1(x - x_1^-)/(\kappa N)} + M \mathrm{e}^{-a_1(x - x_2^-)/(\kappa N)}\right)^2 \mathrm{d}\Omega \right\}^{1/2} \\
&\leqslant \left\{ \int_{x^- \in \Gamma_e^-} \int_{(x^-, y)}^{(x^+, y)} 2\left(M^2 \mathrm{e}^{-2a_1(x - x_1^-)/(\kappa N)}\right) \mathrm{d}x \, \mathrm{d}\Gamma \right. \\
&\qquad \left. + \int_{x^- \in \Gamma_e^-} \int_{(x^-, y)}^{(x^+, y)} 2\left(M^2 \mathrm{e}^{-2a_1(x - x_2^-)/(\kappa N)}\right) \mathrm{d}x \, \mathrm{d}\Gamma \right\}^{1/2} \\
&\leqslant \left\{ \int_{x^- \in \Gamma_e^-} \int_{(x^-, y)}^{(x^+, y)} 2\left(M^2 \mathrm{e}^{-2a_1(x - m'_1 y - k_1)/(\kappa N)}\right) \mathrm{d}x \, \mathrm{d}\Gamma \right. \\
&\qquad \left. + \int_{x^- \in \Gamma_e^-} \int_{(x^-, y)}^{(x^+, y)} 2\left(M^2 \mathrm{e}^{-2a_1(x - m'_2 y - k_2)/(\kappa N)}\right) \mathrm{d}x \, \mathrm{d}\Gamma \right\}^{1/2} \\
&\leqslant \left\{ \int_{x^- \in \Gamma_e^-} M^2 \frac{\kappa N}{a_1} \left(\left(1 - \mathrm{e}^{-2a_1(x^+ - m'_1 y - k_1)/(\kappa N)}\right)\right) \mathrm{d}\Gamma \right. \\
&\qquad \left. + \int_{x^- \in \Gamma_e^-} M^2 \frac{\kappa N}{a_1} \left(\left(1 - \mathrm{e}^{-2a_1(x^+ - m'_2 y - k_2)/(\kappa N)}\right)\right) \mathrm{d}\Gamma \right\}^{1/2} \\
&\leqslant M \left\{ \int_{x^- \in \Gamma_e^-} \frac{2\kappa N}{a_1} \mathrm{d}\Gamma \right\}^{1/2},
\end{aligned} \tag{33}$$

where we have used the fact that for $j \in \{1, 2\}$,

$$1 - \mathrm{e}^{-2a_1(x^+ - x_j^-)} \leqslant 1$$

and

$$\mathrm{e}^{-2a_1(x^+ - x_j^-)} \leqslant 1,$$

for $x^- \in \Gamma_e^-$ and $x^+ \in \Gamma_e^+$. Since $\boldsymbol{a} \cdot \nabla v^h|_{\Omega_e}$ is constant on each Ω_e, it follows from the regularity of the triangulation that

$$M = \sup_{\Gamma_e^-} |\Phi| \leqslant h_a |(\boldsymbol{a} \cdot \nabla v^h)_{\Omega_e}|/a_1, \tag{34}$$

$$\leqslant h_{\Omega_e} |(\boldsymbol{a} \cdot \nabla v^h)_{\Omega_e}|/a_1. \tag{35}$$

Thus the bound obtained for Φ above can be estimated further:

$$\|\Phi\|_{0,\Omega_e} \leqslant \frac{\sqrt{2} M \sqrt{N} \kappa^{1/2} h_{\Omega_e}^{1/2}}{a_1^{1/2}} \leqslant \frac{\sqrt{2}\sqrt{N} \kappa^{1/2} h_{\Omega_e}^{3/2} |(\boldsymbol{a} \cdot \nabla v^h)_{\Omega_e}|}{a_1^{3/2}} \leqslant \frac{\sqrt{2}\sqrt{N} C_2 \kappa^{1/2} h_{\Omega_e}^{1/2} \|\boldsymbol{a} \cdot \nabla v^h\|_{0,\Omega_e}}{a_1^{3/2}}, \tag{36}$$

using the fact that

$$h_{\Omega_e} |(\boldsymbol{a} \cdot \nabla v^h)_{\Omega_e}| \leqslant C_2 \|\boldsymbol{a} \cdot \nabla v^h\|_{0,\Omega_e} \tag{37}$$

for some constant C_2 depending on the minimum angle condition in the triangulation. To see the relation (37), observe that

$$\|\boldsymbol{a} \cdot \nabla v^h\|_{\Omega_e} = |\boldsymbol{a} \cdot \nabla v^h|_{\Omega_e} \left(\int_{\Omega_e} \mathrm{d}\Omega \right)^{1/2} = |\boldsymbol{a} \cdot \nabla v^h|_{\Omega_e} C_2^{-1} h_{\Omega_e}.$$

Since $h_{\Omega_e} = C h_a$ for a non-degenerate triangulation, by the triangle inequality,

$$\|z\|_{0,\Omega_e} \leqslant \|w\|_{0,\Omega_e} + \|\Phi\|_{0,\Omega_e} \leqslant C_3 \left(\frac{\kappa^{1/2} h_a^{1/2}}{a_1^{3/2}} + \frac{\sqrt{2}\kappa}{a_1^2} \right) \|\boldsymbol{a} \cdot \nabla v^h\|_{0,\Omega_e},$$

from (30) and (36), where $C_3 = 2(1 + C_1) + \sqrt{2N} C_2 C$. □

It is crucial that the bounding coefficient above is a multiple of the diffusivity parameter. This fact actually enables us to embed the last term in (26) into the third one in the same equation which is known to be coercive. The next theorem uses this result to establish the coercivity inequality (see [9]).

Theorem 1. *Assume that no edge in the triangulation is aligned with the direction of the flow and that*

$$\kappa \leqslant h_a |\boldsymbol{a}| \min\left\{1, \frac{1}{64C^2}\right\} \tag{38}$$

for all triangles Ω_e in the triangulation. Then

$$a(\bar{v}^h, v^h) \geqslant \sum_e \left(\kappa |v^h|_{1,\Omega_e}^2 + \frac{h_a}{12|\boldsymbol{a}|} \|\boldsymbol{a} \cdot \nabla v^h\|_{0,\Omega_e}^2 \right). \tag{39}$$

Proof. Lemma 1 shows that

$$|(v_\mathrm{b} - v_\mathrm{b}^0, \boldsymbol{a} \cdot \nabla v^h)_{\Omega_e}| \leqslant C \left(\frac{\kappa^{1/2} h_a^{1/2}}{|\boldsymbol{a}|^{3/2}} + \frac{\kappa}{|\boldsymbol{a}|^2} \right) \|\boldsymbol{a} \cdot \nabla v^h\|_{0,\Omega_e}^2. \tag{40}$$

By (26) and (40),

$$\begin{aligned} a(\bar{v}^h, v^h) &= \sum_e \left(\kappa |v^h|^2_{1,\Omega_e} + \frac{h_a}{3|\boldsymbol{a}|} \|\boldsymbol{a} \cdot \nabla v^h\|^2_{0,\Omega_e} + (v_b - v_b^0, \boldsymbol{a} \cdot \nabla v^h)_{\Omega_e} \right) \\ &\geqslant \sum_e \left(\kappa |v^h|^2_{1,\Omega_e} + \frac{h_a}{3|\boldsymbol{a}|} \|\boldsymbol{a} \cdot \nabla v^h\|^2_{0,\Omega_e} - C \left(\frac{\kappa^{1/2} h_a^{1/2}}{|\boldsymbol{a}|^{3/2}} + \frac{\kappa}{|\boldsymbol{a}|^2} \right) \|\boldsymbol{a} \cdot \nabla v^h\|^2_{0,\Omega_e} \right) \\ &\geqslant \sum_e \left(\kappa |v^h|^2_{1,\Omega_e} + \frac{h_a}{12|\boldsymbol{a}|} \|\boldsymbol{a} \cdot \nabla v^h\|^2_{1,\Omega_e} \right), \end{aligned}$$

where we have used (38) for the last inequality and considered the cases $1 \leqslant 64C^2$ and $1 > 64C^2$ separately. $\square$

4. Error estimates

In this section, we study the convergence features of the NOPG method. In Section 3, we have obtained the coercivity inequality (39) under some assumptions on the orientation of the mesh and the relation between κ, $\boldsymbol{a}$ and h_a. The error analysis presented below relies on this stability estimate.

Theorem 2. *Let the solution v^h be the solution of the NOPG method and suppose $v \in H^s(\Omega) \bigcap H^1_0(\Omega)$, $1 < s \leqslant 2$. If*

$$\kappa \leqslant |\boldsymbol{a}| h_a \min \left\{ 1, \frac{1}{64C^2} \right\},$$

then we have the following convergence rates:

$$\sum_e \left(\kappa \|\nabla(v - v^h)\|^2_{0,\Omega_e} + \frac{h_a}{24|\boldsymbol{a}|} \|\boldsymbol{a} \cdot \nabla(v - v^h)\|^2_{0,\Omega_e} \right) \leqslant \sum_e C_{\Omega_e} h_a^{2s-1} |v|^2_{s,\Omega_e}.$$

Proof. Let $\tilde{v}^h$ be the linear interpolant of v, $e_h = \tilde{v}^h - v^h$ and $\eta = \tilde{v}^h - v$. The proof follows the lines of the error analysis of the SUPG method and it is given as follows:

$$\begin{aligned} \sum_e \left(\kappa \|\nabla e_h\|^2_{0,\Omega_e} + \frac{h_a}{12|\boldsymbol{a}|} \|\boldsymbol{a} \cdot \nabla e_h\|^2_{0,\Omega_e} \right) &\leqslant a(\tilde{v}^h - v^h, e_h) = a(\tilde{v}^h - v, e_h) + a(v - v^h, e_h) \\ &= (\eta, \boldsymbol{a} \cdot \nabla e_h) + \kappa(\nabla \eta, \nabla e_h) \\ &\leqslant \sum_e \|\eta\|_{0,\Omega_e} \|\boldsymbol{a} \cdot \nabla e_h\|_{0,\Omega_e} + \sum_e \kappa \|\nabla \eta\|_{0,\Omega_e} \|\nabla e_h\|_{0,\Omega_e} \\ &= \sum_e (h_a \gamma)^{-1/2} \|\eta\|_{0,\Omega_e} (h_a \gamma)^{1/2} \|\boldsymbol{a} \cdot \nabla e_h\|_{0,\Omega_e} \\ &\quad + \sum_e \kappa^{1/2} \|\nabla \eta\|_{0,\Omega_e} \kappa^{1/2} \|\nabla e_h\|_{0,\Omega_e} \\ &\leqslant \sum_e \left(\frac{h_a^{-1} \gamma^{-1}}{2} \|\eta\|^2_{0,\Omega_e} + \frac{h_a \gamma}{2} \|\boldsymbol{a} \cdot \nabla e_h\|^2_{0,\Omega_e} \right. \\ &\quad \left. + \frac{\kappa}{2} \|\nabla \eta\|^2_{0,\Omega_e} + \frac{\kappa}{2} \|\nabla e_h\|^2_{0,\Omega_e} \right), \end{aligned}$$

where we have used the well-known inequality

$$ab \leqslant \frac{a^2}{2} + \frac{b^2}{2}$$

for any real number a and b.

Now choose $\gamma = 1/(12|\boldsymbol{a}|)$. Noting that γ is bounded below away from zero, i.e. $\gamma > C_0 \gg 0$ for some constant C_0, we can subsume the 2nd and 4th terms into the right hand side of the inequality above. Thus we obtain

$$\sum_e \left(\frac{\kappa}{2} \|\nabla e_h\|^2_{0,\Omega_e} + \frac{h_a}{24|\boldsymbol{a}|} \|\boldsymbol{a} \cdot \nabla e_h\|^2_{0,\Omega_e} \right) \leqslant \sum_e \left(\frac{h_a^{-1} C_0}{2} \|\eta\|^2_{0,\Omega_e} + \frac{\kappa}{2} \|\nabla \eta\|^2_{0,\Omega_e} \right). \tag{41}$$

The first term in (41) can be estimated by interpolation theory [3]. For the second term in (41), we remark that the coercivity inequality holds under the assumption that

$$\kappa \leqslant |\boldsymbol{a}| h_a \min \left\{ 1, \frac{1}{64C^2} \right\}$$

and thus, letting $\beta = \min\{1, 1/(64C^2)\}$, we get

$$\frac{\kappa}{2} \|\nabla \eta\|^2_{0,\Omega_e} \leqslant \frac{\beta |\boldsymbol{a}| h_a}{2} \|\nabla \eta\|^2_{0,\Omega_e}. \tag{42}$$

Now the right hand side of (41) can be estimated. The theorem follows by applying the triangle inequality. □

5. Numerical results

In this section we compare the numerical performance of the nearly-optimal Petrov–Galerkin finite element method (NOPG) with the stabilized finite element method (FFH) in Franca et al. [7]. Recall that the design of our implementation of NOPG is based on the advective limit. The following computations test the performance in the *entire range* from diffusion-dominated to advection-dominated cases. We employ both uniform and non-uniform meshes of four-noded quadrilateral elements in all tests.

5.1. Advection skew to the mesh

Consider a constant-coefficient advection–diffusion problem in the unit square $]0,1[\times]0,1[$. There are no distributed sources ($f = 0$). Inhomogeneous Dirichlet data are specified on the inflow boundary so that there is a discontinuity in the inflow Dirichlet data at $\mathbf{x} = (0, 0.475)$, with homogeneous Neumann outflow conditions (Fig. 7). We use uniform and non-uniform (Fig. 8) meshes with 20×20 elements.

The discontinuity is propagated into the domain creating an internal layer. Here, the element Péclet number is $(|\boldsymbol{a}|h)/2\kappa = 2.5 \times 10^4$. The problem is solved at $\theta = \pi/6$, $\pi/4$, and $\pi/3$. For example, solutions on the uniform mesh at $\theta = \pi/6$ are shown in Fig. 9. The NOPG solution exhibits much better performance for these problems with discontinuities, particularly when the flow is along element diagonals (Fig. 10).

Results for the non-uniform mesh are shown in Fig. 11. Both methods retain the main features of solutions obtained on the uniform mesh.

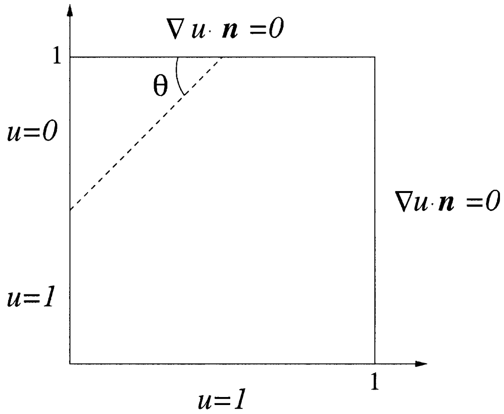

Fig. 7. Statement of Problem 5.1.

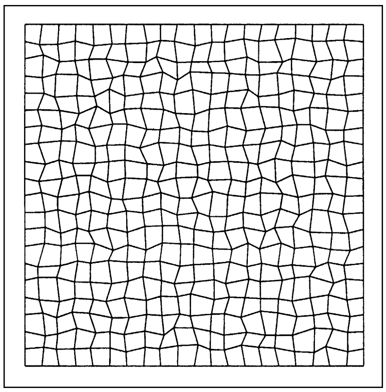

Fig. 8. 20×20 non-uniform mesh employed in Problems 5.1 and 5.2.

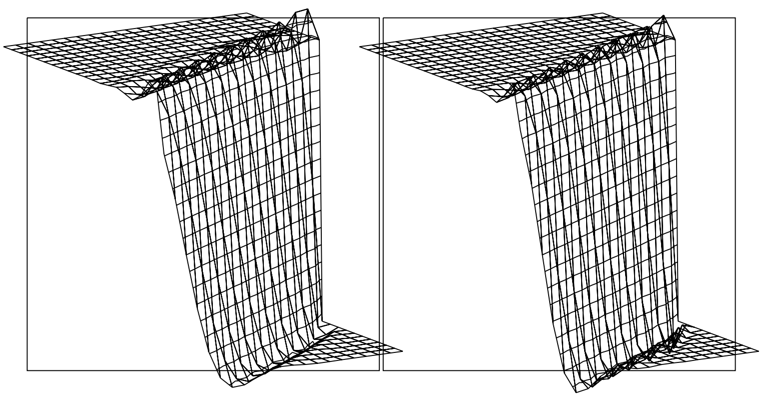

Fig. 9. Solutions of Problem 5.1 on the uniform mesh at $\theta = \pi/6$: FFH (left), and NOPG (right).

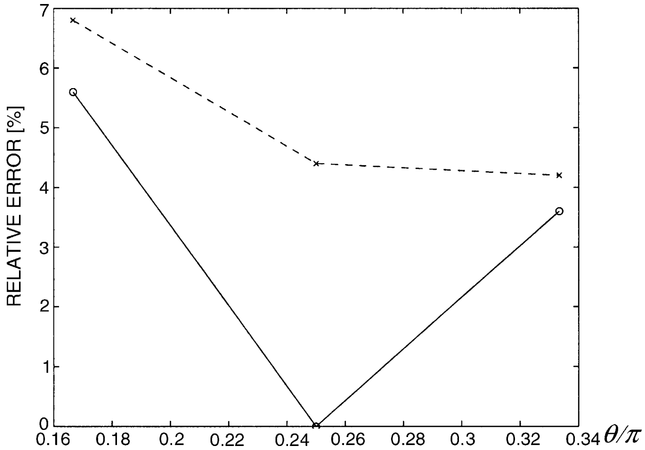

Fig. 10. L_2 error (%) for the uniform mesh in Problem 5.1 relative to the nodal interpolant: FFH (- -) and NOPG (—).

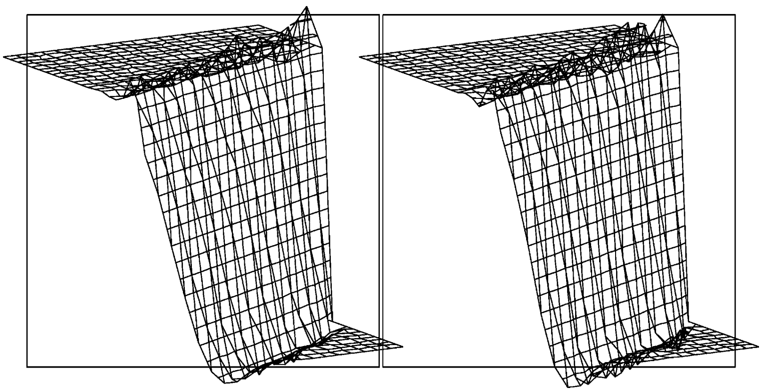

Fig. 11. Solutions of Problem 5.1 on the non-uniform mesh at $\theta = \pi/6$: FFH (left), and NOPG (right).

5.2. Advection skew to the mesh with outflow boundary layers

The outflow conditions of Problem 5.1 are changed to homogeneous Dirichlet conditions, leading to outflow boundary layers [4,7]. Note that the interpolant now accounts for the outflow boundary layers. The problem is solved at $\theta = \pi/6$, $\pi/4$, and $\pi/3$. For example, solutions on the uniform mesh at $\theta = \pi/6$ are shown in Fig. 12. The outflow boundary layers may not represent typical physical configurations, but they are numerically challenging. The performance of both method is similar to the previous case yet with larger relative errors; see Fig. 13. The main characteristics of the solutions are still retained when the non-uniform mesh is employed (Fig. 14).

5.3. Transport in a rotating flow field

Consider a homogeneous Dirichlet advection–diffusion problem [7,12] in the unit square (centered at the origin, Fig. 15). There are no distributed sources ($f = 0$), $\kappa = 10^{-6}$, and $\boldsymbol{a}^{\mathrm{T}} = \langle -y, x \rangle$ representing a rotating

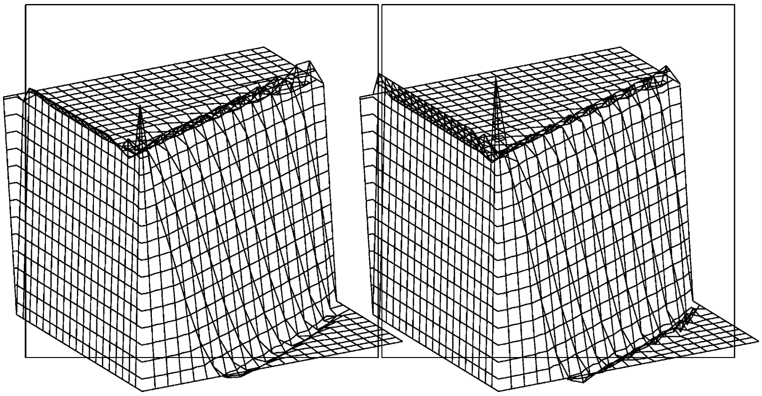

Fig. 12. Solutions of Problem 5.2 on the uniform mesh at $\theta = \pi/6$: FFH (left), and NOPG (right).

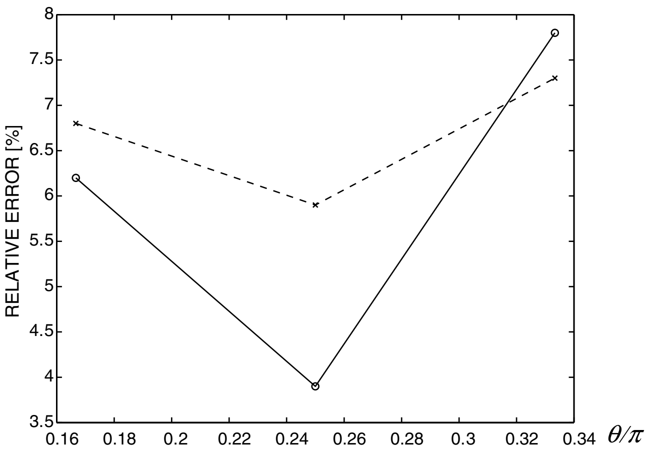

Fig. 13. L_2 error (%) for the uniform mesh in Problem 5.2 relative to the nodal interpolant: FFH (- -) and NOPG (—).

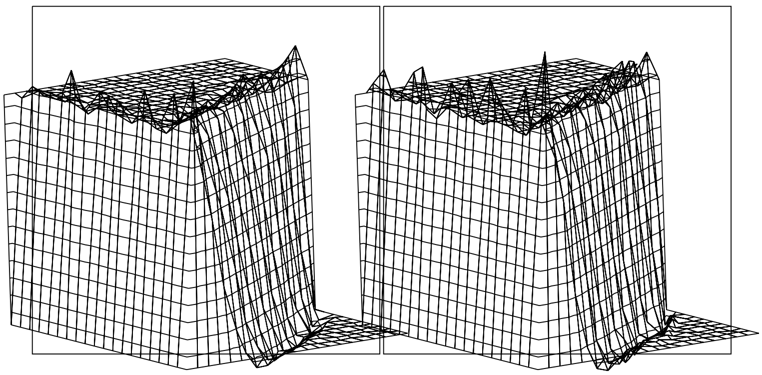

Fig. 14. Solutions of Problem 5.2 on the non-uniform mesh at $\theta = \pi/6$: FFH (left), and NOPG (right).

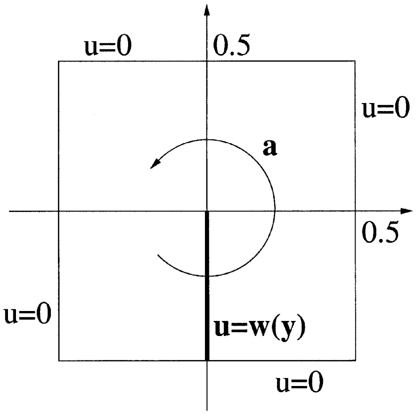

Fig. 15. Statement of Problem 5.3.

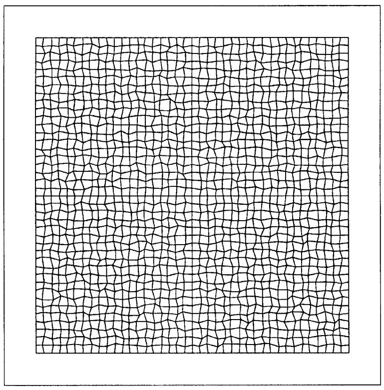

Fig. 16. 40×40 Non-uniform mesh employed in Problem 5.3.

velocity field. There is an internal boundary along the negative y-axis, with the boundary condition $u(0,y) = w(y)$, where

$$w(y) = \tfrac{1}{2}[\cos(4\pi y + \pi) + 1], \quad -0.5 \leqslant y \leqslant 0. \tag{43}$$

The reference solution is obtained by FFH on a uniform mesh of 200×200 elements. The tests are performed on a uniform and a non-uniform mesh (Fig. 16) of 40×40 elements. Velocity is taken to be constant inside each element and its value is assigned at the center of the element.

Solutions on the uniform mesh are shown in Fig. 17. Table 1 shows the relative error of the uniform mesh, measured in the L_2 norm. The NOPG solution is better than FFH, even though the design of the NOPG method implemented herein is based on the advective limit, while this problem contains diffusion-dominated regions.

Results for the non-uniform mesh are shown in Fig. 18. Both methods are robust and retain the main features of solutions obtained on the uniform mesh.

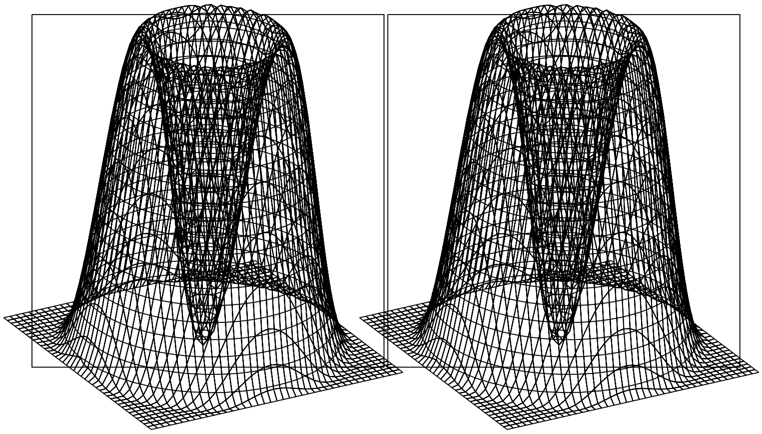

Fig. 17. Solutions of Problem 5.3 on the uniform mesh: FFH (left), and NOPG (right).

Table 1
L_2 Relative errors (%) for the uniform mesh in Problem 5.3

	Relative to nodal interpolant
FFH	0.484
NOPG	0.353

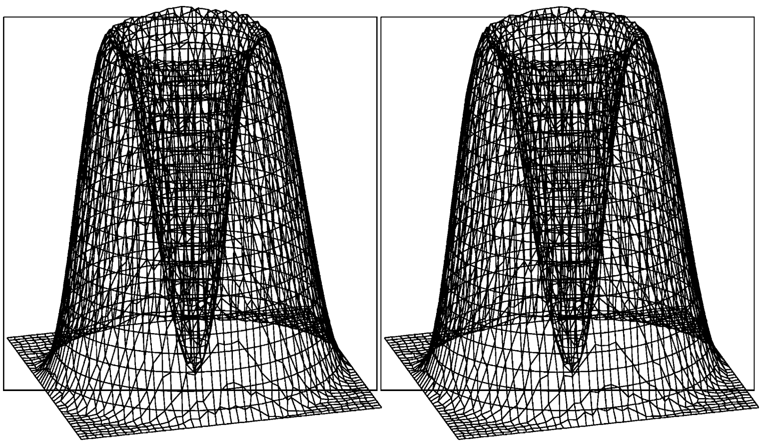

Fig. 18. Solutions of Problem 5.3 on the non-uniform mesh: FFH (left), and NOPG (right).

6. Conclusion

In this paper we employ the nearly-optimal Petrov–Galerkin method to improve finite element computation of convection-dominated transport phenomena. By the construction of the NOPG weighting functions, this method approximates optimality in the H^1 semi-norm, which provides high coarse-mesh accuracy that guarantees good performance of the computation at any mesh refinement. The NOPG method is related to residual-free bubbles in certain settings.

The design of the NOPG method for convection–diffusion in this paper is based on consideration of the advective limit. The resulting method is applicable to the entire admissible range of problem parameters.

We investigate the stability properties of this method, ultimately deriving a coercivity inequality. The convergence features of the NOPG method for convection–diffusion are studied in an error analysis that is based on the stability estimates. The proposed method compares favorably to the performance of an established technique on several numerical tests.

Acknowledgements

The authors would like to thank Paul Barbone, Leo Franca, Saulo Oliveira, and Martin Stynes for helpful discussions. The second author gratefully acknowledges support from the Izmir Institute of Technology, Izmir, Turkey, and the Turkish Scientific and Technical Research Council (TUBITAK) grant under the NATO-D Visiting Scholar Program.

References

[1] I. Babuška, J.M. Melenk, The partition of unity method, Int. J. Numer. Methods Engrg. 40 (4) (1997) 727–758.

[2] P.E. Barbone, I. Harari, Nearly H^1-optimal finite element methods, Comput. Methods Appl. Mech. Engrg. 190 (43–44) (2001) 5679–5690.

[3] S. Brenner, L. Scott, The Mathematical Theory of Finite Element Methods, Springer-Verlag, New York, 1994.

[4] F. Brezzi, L.P. Franca, A. Russo, Further considerations on residual-free bubbles for advective–diffusive equations, Comput. Methods Appl. Mech. Engrg. 166 (1–2) (1998) 25–33.

[5] A.N. Brooks, T.J.R. Hughes, Streamline upwind/Petrov–Galerkin formulations for convection dominated flows with particular emphasis on the incompressible Navier-Stokes equations, Comput. Methods Appl. Mech. Engrg. 32 (1–3) (1982) 199–259.

[6] C. Farhat, I. Harari, L.P. Franca, The discontinuous enrichment method, Comput. Methods Appl. Mech. Engrg. 190 (48) (2001) 6455–6479.

[7] L.P. Franca, S.L. Prey, T.J.R. Hughes, Stabilized finite element methods. I. Application to the advective–diffusive model, Comput. Methods Appl. Mech. Engrg. 95 (2) (1992) 253–276.

[8] L.P. Franca, A. Nesliturk, On a two-level finite element method for the incompressible Navier-Stokes equations, Int. J. Numer. Methods Engrg. 52 (2001) 433–453.

[9] L.P. Franca, A. Nesliturk, M. Stynes, On the stability of residual-free bubbles for convection-diffusion problems and their approximation by a two-level finite element method, Comput. Methods Appl. Mech. Engrg. 166 (1–2) (1998) 35–49.

[10] I. Harari, L.P. Franca, S.P. Oliveira, Streamline design of stability parameters for advection–diffusion problems, J. Comput. Phys. 171 (1) (2001) 115–131.

[11] T.J.R. Hughes, Multiscale phenomena: Green's functions, the Dirichlet-to-Neumann formulation, subgrid scale models, bubbles and the origins of stabilized methods, Comput. Methods Appl. Mech. Engrg. 127 (1–4) (1995) 387–401.

[12] T.J.R. Hughes, A.N. Brooks, A multidimensional upwind scheme with no crosswind diffusion, in: T.J.R. Hughes (Ed.), Finite Element Methods For Convection Dominated Flows, AMD, vol. 34, ASME, New York, 1979, pp. 19–35.

[13] T.J.R. Hughes, L.P. Franca, G.M. Hulbert, A new finite element formulation for computational fluid dynamics. VIII. The Galerkin/least-squares method for advective–diffusive equations, Comput. Methods Appl. Mech. Engrg. 73 (2) (1989) 173–189.

[14] J.M. Melenk, I. Babuška, The partition of unity method finite element method: basic theory and applications, Comput. Methods Appl. Mech. Engrg. 139 (1–4) (1996) 289–314.

[15] A.A. Oberai, P.M. Pinsky, A multiscale finite element method for the Helmholtz equation, Comput. Methods Appl. Mech. Engrg. 154 (3–4) (1998) 281–297.

[16] M.H. Protter, H.F. Weinberger, Maximum Principles in Differential Equations, Prentice-Hall, New Jersey, 1967.

[17] T. Strouboulis, I. Babuška, K. Copps, The design and analysis of the generalized finite element method, Comput. Methods Appl. Mech. Engrg. 181 (1–3) (2000) 43–69.